Universal Scaling of the Conductivity at the Superfluid-Insulator Phase Transition

Jurij Šmakov and Erik Sørensen

Department of Physics and Astronomy, McMaster University, Hamilton, Ontario L8S 4M1, Canada

(Received 30 May 2005; published 27 October 2005)

The scaling of the conductivity at the superfluid-insulator quantum phase transition in two dimensions is studied by numerical simulations of the Bose-Hubbard model. In contrast to previous studies, we focus on properties of this model in the experimentally relevant thermodynamic limit at finite temperature T. We find clear evidence for *deviations* from ω_k scaling of the conductivity towards ω_k/T scaling at low Matsubara frequencies ω_k. By careful analytic continuation using Padé approximants we show that this behavior carries over to the real frequency axis where the conductivity scales with ω/T at small frequencies and low temperatures. We estimate the universal dc conductivity to be $\sigma^* = 0.45(5)Q^2/h$, distinct from previous estimates in the $T = 0$, $\omega/T \gg 1$ limit.

DOI: 10.1103/PhysRevLett.95.180603 PACS numbers: 05.60.Gg, 02.70.Ss, 05.70.Jk

The nontrivial properties of materials in the vicinity of quantum phase transitions [1] (QPTs) are an object of intense theoretical [1–3] and experimental studies. The effect of quantum fluctuations driving the QPTs is especially pronounced in low-dimensional systems, such as high-temperature superconductors and two-dimensional (2D) electron gases, exhibiting the quantum Hall effect. Particularly valuable are theoretical predictions of the behavior of the dynamical response functions, such as the optical conductivity and the dynamic structure factor, since they allow for direct comparison of the theoretical results with experimental data. It was pointed out by Damle and Sachdev [2] that at the quantum-critical coupling the scaled dynamic conductivity $T^{(2-d)/z}\sigma(\omega, T)$ at low frequencies and temperatures is a function of the single variable $\hbar\omega/k_BT$:

$$\sigma(\omega/T, T \to 0) = (k_BT/\hbar c)^{(d-2)/z}\sigma_Q\Sigma(\hbar\omega/k_BT). \quad (1)$$

Here $\sigma_Q = Q^2/h$ is the conductivity "quantum" ($Q = 2e$ for the models we consider), $\Sigma(x \equiv \hbar\omega/k_BT)$ is a universal dimensionless scaling function, c a nonuniversal constant, and z the dynamical critical exponent. For $d = 2$ the exponent vanishes, leading to a purely universal conductivity [4], depending only on frequency ω, measured against a characteristic time $\hbar\beta$ set by finite temperature T as $\hbar\omega/k_BT$. Once $\hbar\omega/k_BT \gg 1$, for *fixed* T, the system no longer "feels" the effect of finite temperature and it is natural to expect that at such high ω a crossover to a temperature-independent regime will take place [3], so that $\sigma(\omega, T) \sim \sigma(\omega)$ with $\sigma(\omega)$ decaying at high frequencies as $1/\omega^2$ [2]. Deviations from scaling of σ with ω therefore signal that temperature effects have become important. Note that the predicted universal behavior occurs for *fixed* ω/T as $T \to 0$. The physical mechanisms of transport are predicted [2] to be quite distinct in the different regimes determined by the value of the scaling variable x: hydrodynamic, collision dominated for $x \ll 1$, and collisionless, phase coherent for $x \gg 1$ with $\Sigma = \Sigma(\infty)$ largely independent of x in $d = 2$ and σ independent of T [2,5].

Intriguingly, early numerical studies [6–9] of QPTs in model systems have failed to observe scaling with $\hbar\omega/k_BT$. The results of the experiments seeking to verify the scaling hypothesis are ambiguous as well. Some of them, performed at the 2D quantum Hall transitions [10] and 3D metal-insulator transitions [11], appear to support it. Others either note the absence of scaling [12] or suggest a different scaling form [13]. While the discrepancy between theory and experiment may be attributed to the unsuitable choice of the measurement regime [2], typically leading to $\hbar\omega/k_BT \gg 1$, there is no good reason why the predicted scaling would not be observable in numerical simulations if careful extrapolations first to $L \to \infty$ and then $T \to 0$ for fixed ω/T are performed.

Our primary goal is to resolve this controversy by performing precise numerical simulations of the frequency-dependent conductivity at finite temperatures in the vicinity of the 2D QPT, exploiting recent algorithmic advances to access larger system sizes and a wider temperature range. After the extrapolation of the results to the thermodynamic and $T = 0$ limits and careful analytic continuation, we are able to demonstrate how the predicted universal behavior of the conductivity may indeed be revealed.

We consider the 2D Bose-Hubbard (BH) model with the Hamiltonian $\mathcal{H}_{\mathrm{BH}} = \mathcal{H}_0 + \mathcal{H}_1$, where the first term describes the noninteracting soft core bosons hopping via the nearest-neighbor links of a 2D square lattice, and the second one includes the Hubbard-like on-site interactions:

$$\mathcal{H}_0 = -t\sum_{\mathbf{r},\delta}(b^\dagger_{\mathbf{r}}b_{\mathbf{r}+\delta} + b^\dagger_{\mathbf{r}+\delta}b_{\mathbf{r}}) - \mu\sum_{\mathbf{r}} n_{\mathbf{r}}, \quad (2)$$

$$\mathcal{H}_1 = \frac{U}{2}\sum_{\mathbf{r}} n_{\mathbf{r}}(n_{\mathbf{r}} - 1). \quad (3)$$

Here $\delta = \mathbf{x}, \mathbf{y}$, $n_{\mathbf{r}} = b^\dagger_{\mathbf{r}}b_{\mathbf{r}}$ is the particle number operator on site $\mathbf{r}$, and $b^\dagger_{\mathbf{r}}$, $b_{\mathbf{r}}$ are the boson creation and annihilation

operators at site $\mathbf{r}$. Model parameters include the hopping constant t, Hubbard repulsion U, and chemical potential μ. The mean-field ground state phase diagram of this model (Fig. 1) displays a number of Mott-insulating lobes with fixed integer boson density at low Zt/U ($Z = 4$ is the lattice coordination number). As the hopping t is increased or μ is varied, a QPT to a superfluid (SF) phase takes place. We concentrate on the QPT occurring at the tip of the Mott lobe along the path of constant μ, distinct from the generic one occurring elsewhere along the phase boundary [14].

The numerical simulations of $\mathcal{H}_{\mathrm{BH}}$ were performed using the stochastic series expansion (SSE) technique with directed loop updates [15,16], which allowed us to directly evaluate the relevant correlation functions without the need to discretize or numerically integrate over the imaginary time. We have also employed an alternative $(2 + 1)$-dimensional classical representation [7,17] of $\mathcal{H}_{\mathrm{BH}}$ in terms of link-current variables describing the total bosonic current $\mathbf{J} = (J^x, J^y, J^\tau)$ defined on a discrete $L \times L \times L_\tau$ space-time lattice ($L_\tau \Delta_\tau = \hbar\beta$):

$$\mathcal{H}_V = \frac{1}{K} \sum_{(\mathbf{r},\tau)} \left[\frac{1}{2} \mathbf{J}^2_{(\mathbf{r},\tau)} - \mu J^\tau_{(\mathbf{r},\tau)} \right]. \tag{4}$$

$\mathbf{J}$ has to be conserved and is therefore divergence free, $\boldsymbol{\nabla} \cdot \mathbf{J} = 0$. The link-current variables take on integer values $J^{x,y,\tau} = 0, \pm 1, \pm 2, \ldots$ and denote the deviation of the particle number from its mean, so the transition corresponds to $\mu = 0$. K is the effective temperature, varying like t/U in $\mathcal{H}_{\mathrm{BH}}$. The model defined by $\mathcal{H}_V$ has been studied in the past using a very efficient directed geometrical worm algorithm [18], and its critical point at $\mu = 0$ has been determined [18] to be $K_c = 0.33305(5)$. A drawback of this representation is that the time direction is discrete, imposing an ultraviolet frequency cutoff of data at $\omega_c = 1/\Delta\tau$, in contrast to SSE, where there is no such problem. The two numerical approaches are therefore largely complementary. These advanced techniques allowed us to simulate lattices of linear sizes up to $L = 30$ and inverse temperatures up to $\beta = 10$ using SSE for $\mathcal{H}_{\mathrm{BH}}$, and $L = 256$, $L_\tau = 64$ using the directed geometrical worm algorithm for $\mathcal{H}_V$.

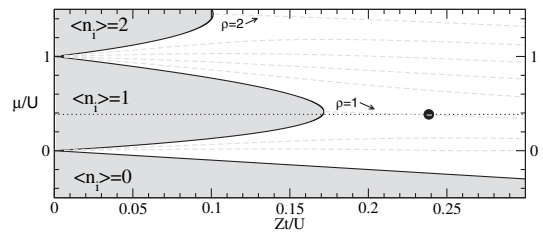

FIG. 1. Mean-field ground state phase diagram of the 2D Bose-Hubbard model. Shaded areas are the Mott-insulating phases. Dashed lines are constant density profiles in steps of 0.2. ● indicates the location of QCP at the tip of Mott lobe as determined by SSE simulations along the dotted line.

Performing SSE simulations of $\mathcal{H}_{\mathrm{BH}}$ we first precisely locate the quantum-critical point (QCP) for fixed μ/U at the tip of the first Mott lobe. This transition belongs to the $(2 + 1)$D XY universality class with a dynamical critical exponent $z = 1$ [14]. In the vicinity of the QCP the SF density ρ_s and compressibility κ are expected to obey the scaling relations

$$\rho_s = L^{2-d-z} Y_1(\delta L^{1/\nu}, \beta L^{-z}), \tag{5}$$

$$\kappa = L^{z-d} Y_2(\delta L^{1/\nu}, \beta L^{-z}). \tag{6}$$

Here ν is the correlation length critical exponent, $\beta = 1/k_B T$, $\delta = |t - t_c|$, and $Y_{1,2}(x, y)$ are the two-variable scaling functions. For a fixed aspect ratio βL^{-z} plots of the $L\rho_s$ and $L\kappa$ should then intersect at the critical point $\delta = 0$. Results of such a calculation at constant $\mu_c/U = 0.375$ are presented in Fig. 2, from which we determine $Zt_c/U = 0.2385(5)$, $\nu = 0.66(5)$. The position of the QCP and the shape of the phase boundary in its vicinity is consistent with previous simulations [19] and strong-coupling perturbation theory [20].

To analyze the behavior of the zero-momentum conductivity in the vicinity of the QCP we employ the relation between the dynamic conductivity $\sigma(\omega)$ and the Fourier transform $\Lambda_{xx}(\omega)$ of the time-dependent current-current correlation function (CCCF) established by the Kubo formula [21,22]. In SSE the real-time CCCF required to determine $\Lambda_{xx}(\omega)$ is not directly accessible. Instead, the standard approach is to measure the CCCF $\Lambda_{xx}(\tau) = \langle j_x(\tau) j_x(0) \rangle$ on the imaginary time axis, calculate its Fourier transform $\Lambda_{xx}(i\omega_k)$ as a function of the Matsubara frequencies $\omega_k \equiv 2\pi k/\beta$, and analytically continue the result to real frequencies [8,9,22]. Here and below we adopt a unit system in which both Q and $\hbar$ are unity, and $j_x(\tau)$ is the Heisenberg representation of the current operator $j_x = it[b^\dagger_{\mathbf{r}+\mathbf{x}} b_{\mathbf{r}} - b^\dagger_{\mathbf{r}} b_{\mathbf{r}+\mathbf{x}}]$. We have:

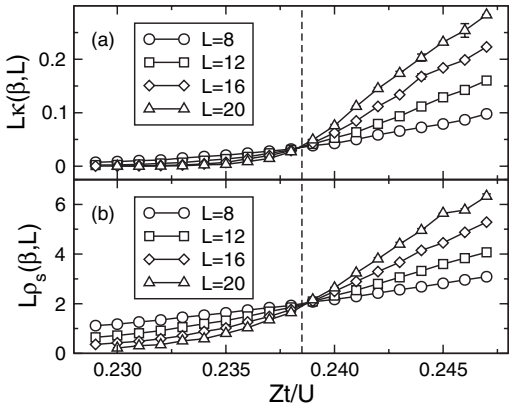

FIG. 2. The compressibility (a) and SF density (b) vs Zt/U at fixed $\mu/U = 0.375$ and aspect ratio $\beta L^{-z} = 0.5$. The dashed vertical line is drawn at $Zt_c/U = 0.2385$. Error bars are displayed only if larger than the symbol size.

$$\sigma(i\omega_k)/(2\pi\sigma_Q) = \frac{\langle -k_x\rangle - \Lambda_{xx}(i\omega_k)}{\omega_k} \equiv \frac{\rho(i\omega_k)}{\omega_k}. \quad (7)$$

Here $\langle -k_x\rangle$ is the kinetic energy per link and $\rho(i\omega_k)$ is the frequency-dependent stiffness. To measure $\Lambda_{xx}(i\omega_k)$ we note that $\Lambda_{xx}(\tau)$ may be expressed in terms of the correlation functions $\Lambda^{\gamma\nu}_{xx}(\mathbf{r},\tau) = \langle K^{\gamma}_x(\mathbf{r},\tau)K^{\nu}_x(\mathbf{0},0)\rangle$ of operators $K^{+}_x(\mathbf{r},\tau) = tb^{\dagger}_{\mathbf{r}+\mathbf{x}}(\tau)b_{\mathbf{r}}(\tau)$ and $K^{-}_x(\mathbf{r},\tau) = tb^{\dagger}_{\mathbf{r}}(\tau)b_{\mathbf{r}+\mathbf{x}}(\tau)$, which may be estimated efficiently in SSE [15]. Remarkably, it is possible to analytically perform the Fourier transform with respect to τ yielding

$$\Lambda^{\gamma\nu}_{xx}(\mathbf{r},\omega_k) = \left\langle \frac{1}{\beta}\sum_{m=0}^{n-2} \bar{a}_{mn}(\omega_k) N(\nu,\gamma;m)\right\rangle, \quad (8)$$

where $N(\nu,\gamma;m)$ is the number of times the operators $K^{\gamma}(\mathbf{r})$ and $K^{\nu}(\mathbf{0})$ appear in the SSE operator sequence separated by m operator positions, and n is the expansion order. The coefficients $\bar{a}_{mn}(\omega_k)$ are given by the degenerate hypergeometric (Kummer) function: $\bar{a}_{mn}(\omega_k) = {}_1F_1(m+1, n; -i\beta\omega_k)$. This expression and (8) allow us to directly evaluate $\Lambda_{xx}(\mathbf{r},\omega_k)$ as a function of Matsubara frequencies, eliminating any errors associated with the discretization of the imaginary time interval. Analogously, in the link-current representation $\rho(i\omega_k)$ can be calculated [7], and the conductivity can be obtained from Eq. (7).

In Fig. 3 we show results for $\sigma(i\omega_k)$ versus ω_k obtained using the geometrical worm algorithm on $\mathcal{H}_V$ at K_c [Fig. 3(a)] and by SSE simulations at t_c, μ_c of $\mathcal{H}_{\mathrm{BH}}$ [Fig. 3(c)]. In both cases the results have been extrapolated to the thermodynamic limit $L \to \infty$ at fixed β. As evident from Fig. 3(a), the results *deviate* from scaling with ω_k at small ω_k and more significantly so at higher temperatures (small L_τ). These deviations are also visible in the continuous time SSE data in Fig. 3(c), demonstrating that they cannot be attributed to time discretization errors. Similar deviations have been noted previously [6,7] but were *not* analyzed at fixed β. Since the deviations persist in the $L \to \infty$ limit at fixed β, they may only be interpreted as *finite* T effects. Expecting a crossover to ω_k/T scaling at small ω_k, we plot our results versus ω_k/T in Fig. 3(d). For $L_\tau \geq 32$, $\sigma(\omega_1/T)$ is already *independent* of T (L_τ). In fact, as shown in Fig. 3(d), for $\omega_{1\ldots5}$, $\sigma(\omega_k/T, T)$ can unambiguously be extrapolated to a *finite* $\sigma(\omega_k/T, T \to 0) \sim \Sigma(x)$ limit. This fact is a clear indication that ω_k/T scaling indeed occurs as $T \to 0$. Tentatively, for increasing ω_k/T, $\sigma(\omega_k/T, T \to 0)$ appears to reach a constant value of roughly $0.33\sigma_Q \sim \Sigma(\infty)$ in excellent agreement with theoretical estimates [2,23]. We note that deviations from ω_k scaling appear to be largely *absent* in simulations of $\mathcal{H}_{\mathrm{BH}}$ with disorder [7,8]. However, at this QCP the dynamical critical exponent is different ($z = 2$). As is evident from the size of the error bars in Fig. 3, simulations of $\mathcal{H}_V$ are much more efficient than the SSE simulations directly on $\mathcal{H}_{\mathrm{BH}}$. In the following analytic continuation we therefore use the SSE data mostly as a consistency check.

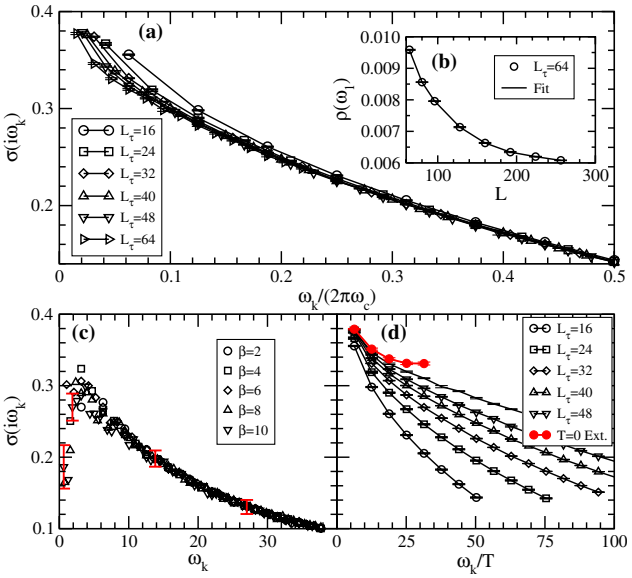

FIG. 3 (color online). The conductivity $\sigma(\omega_k)$ in units of σ_Q vs Matsubara frequency ω_k/ω_c as obtained from $\mathcal{H}_V$ (a). All results have been extrapolated to the thermodynamic limit $L \to \infty$ using the scaling form $f(L) = a + b\exp(-L/\xi)/\sqrt{L}$ [27] by calculating $\rho(\omega_k)$ at fixed L_τ using 9 lattice sizes from $L = L_\tau \ldots 4L_\tau$ as shown in (b). $\sigma(\omega_k)$ in units of σ_Q vs Matsubara frequency ω_k as obtained from SSE calculations of $\mathcal{H}_{\mathrm{BH}}$, with some typical error bars shown. All results have been extrapolated to the thermodynamic limit by calculating $\Lambda_{xx}(\omega_k)$ for fixed β using 5 lattice sizes $L = 12, \ldots, 30$ (c). Scaling plot of the conductivity data from (a) vs ω_k/T. ● denotes extrapolations to $T \to 0$ ($L_\tau \to \infty$) at fixed ω_k/T using: $f(L_\tau) = c + d\exp(-L_\tau/\xi_\tau)/\sqrt{L_\tau}$ [27] (d).

Our results on the imaginary frequency axis are limited by the lowest Matsubara frequency, $\omega_1 = 2\pi k_B T/\hbar$. However, the information about the behavior of $\sigma'(\omega) \equiv \mathrm{Re}\sigma(\omega)$ at low ω is embedded in values of the CCCF at all Matsubara frequencies, allowing us to determine it. In order to study the ω/T scaling predicted for the hydrodynamic collision-dominated regime [2] $\hbar\omega/k_B T \ll 1$, we have attempted analytic continuations of $\rho(i\omega_k)$ to obtain $\sigma'(\omega)$ at real frequencies. SSE results for $\mathcal{H}_{\mathrm{BH}}$ were analytically continued using the Bryan maximum entropy (ME) method [24] with flat initial image. For the results obtained for the link-current model $\mathcal{H}_V$ we use a method that should be most sensitive to low frequencies $\omega/\omega_c < 1$ or $\Sigma(x \ll 1)$. We fit the extrapolated low frequency part (first 10–15 Matsubara frequencies) of $\rho(i\omega_k)$ to a 6th-order polynomial. The resulting 6 coefficients are then used to obtain a (3, 3) Padé approximant using standard techniques [25]. This approximant is then used for the analytic continuation of ρ by $i\omega_k \to \omega + i\delta$. Resulting real frequency conductivities $\sigma'(\omega)$ are displayed in Fig. 4(a) versus ω/ω_c. The typical SSE data are plotted versus $\omega/10$ and are only shown for $L = 20$, $\beta = 10$.

The results for $\mathcal{H}_V$ show a broadened peak as $\omega \to 0$, due to inelastic scattering, followed by a second peak nicely consistent in height and width with the SSE data.

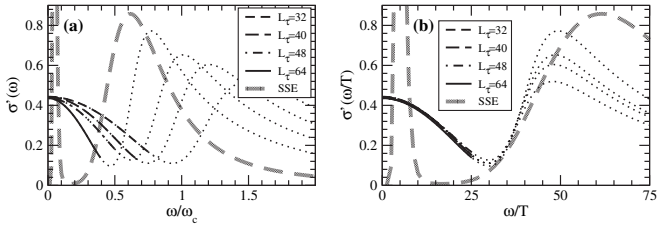

FIG. 4. The real part of the conductivity σ' at the critical coupling in units of σ_Q. The data marked L_τ, plotted vs ω/ω_c, were obtained using $\mathcal{H}_V$, combined with the analytic continuation of $\rho(\omega/\omega_c)$ as explained in the text. Results for $\omega/\omega_c \gtrsim 1/2$ are denoted by dotted lines. The data marked SSE, plotted vs $\omega/10$, were obtained by direct SSE simulations of $\mathcal{H}_{\mathrm{BH}}$ with $L = 20$, $\beta = 10$ and subsequent maximum entropy analysis (a). Results as a function of ω/T (b).

The SSE data also display a high narrow peak at very low frequencies, whose position and shape are unstable with respect to the choice of the initial image and MaxEnt parameters. This is clearly an artifact of the method; however, its presence is indicative of the tendency to accumulate the weight at very low frequencies, in qualitative agreement with $\mathcal{H}_V$ result. The subsequent falloff in the conductivity at high frequencies is physically consistent, but its functional form depends on the Padé approximant used. For $\omega/\omega_c \gtrsim 1/2$, we expect the analytic continuation of the data for $\mathcal{H}_V$ to become sensitive to the order of the approximant used and we therefore indicate the results in this regime by dotted lines only. We note that results at *all* temperatures yield the same dc conductivity $\sigma^\star = 0.45(5)\sigma_Q$, theoretically predicted [4] to be universal. Because of the very different scaling procedure this result differs from previous numerical result $\sigma^\star = 0.285(20)\sigma_Q$ on the same model [6] in the $T = 0$ limit. It also differs significantly from a theoretical estimate [2], $\sigma^* = 1.037\sigma_Q$, valid to leading order in $\epsilon = 3 - d$. Remarkably, our result for the dc conductivity is very close to the one obtained in Ref. [8] for the phase transition in the disordered Bose-Hubbard model. Experimental results indicate a value close to unity [26]; however, it was previously observed [7] that long-range Coulomb interactions, impossible to include in the present study, tend to increase σ considerably. The same data are shown versus ω/T in Fig. 4(b). Notably, when using this parametrization ω_c *cancels out* and all our data follow the *same* functional form. The scaling with ω/T at low frequencies is now immediately apparent, with a surprisingly wide low ω/T peak. The width of this peak is consistent with the data in Fig. 3(d). Furthermore, on the same ω/T scale the continuous time SSE data for $\mathcal{H}_{\mathrm{BH}}$ and the results for $\mathcal{H}_V$ qualitatively agree.

In summary, we have demonstrated that by doing a very careful data analysis it is possible to observe the theoretically predicted universal ω/T scaling at the 2D superfluid-insulator transition. We have also estimated the universal dc conductivity at this transition and found that it differs significantly from existing numerical and theoretical estimates.

We thank S. Sachdev, S. Girvin, and A. P. Young for valuable comments and critical remarks. Financial support from SHARCNET, NSERC, and CFI is gratefully acknowledged. All calculations were done at the SHARCNET facility at McMaster University.

[1] J. Hertz, Phys. Rev. B **14**, 1165 (1976); A. J. Millis, Phys. Rev. B **48**, 7183 (1993); S. Sachdev, *Quantum Phase Transitions* (Cambridge University Press, Cambridge, England, 2001); M. Vojta, Rep. Prog. Phys. **66**, 2069 (2003).
[2] K. Damle and S. Sachdev, Phys. Rev. B **56**, 8714 (1997).
[3] S. L. Sondhi *et al.*, Rev. Mod. Phys. **69**, 315 (1997).
[4] M. P. A. Fisher, G. Grinstein, and S. M. Girvin, Phys. Rev. Lett. **64**, 587 (1990).
[5] S. Sachdev, Phys. Rev. B **55**, 142 (1997).
[6] M.-C. Cha *et al.*, Phys. Rev. B **44**, 6883 (1991).
[7] E. S. Sørensen *et al.*, Phys. Rev. Lett. **69**, 828 (1992); M. Wallin *et al.*, Phys. Rev. B **49**, 12 115 (1994).
[8] G. G. Batrouni *et al.*, Phys. Rev. B **48**, 9628 (1993).
[9] R. T. Scalettar, N. Trivedi, and C. Huscroft, Phys. Rev. B **59**, 4364 (1999).
[10] L. W. Engel *et al.*, Phys. Rev. Lett. **71**, 2638 (1993).
[11] H.-K. Lee *et al.*, Phys. Rev. Lett. **80**, 4261 (1998); Science **287**, 633 (2000).
[12] N. Q. Balaban, U. Meirav, and I. Bar-Joseph, Phys. Rev. Lett. **81**, 4967 (1998).
[13] Y. S. Lee *et al.*, Phys. Rev. B **66**, 041104(R) (2002).
[14] M. P. A. Fisher *et al.*, Phys. Rev. B **40**, 546 (1989).
[15] A. W. Sandvik, J. Phys. A **25**, 3667 (1992).
[16] O. F. Syljuåsen and A. W. Sandvik, Phys. Rev. E **66**, 046701 (2002); O. F. Syljuåsen, *ibid.* **67**, 046701 (2003).
[17] M. P. A. Fisher and D. H. Lee, Phys. Rev. B **39**, 2756 (1989).
[18] F. Alet and E. S. Sørensen, Phys. Rev. E **67**, 015701(R) (2003); **68**, 026702 (2003).
[19] W. Krauth and N. Trivedi, Europhys. Lett. **14**, 627 (1991).
[20] J. K. Freericks and H. Monien, Phys. Rev. B **53**, 2691 (1996); N. Elstner and H. Monien, *ibid.* **59**, 12 184 (1999).
[21] G. D. Mahan, *Many-Particle Physics* (Plenum, New York, 1990), 2nd ed..
[22] D. J. Scalapino, S. R. White, and S. Zhang, Phys. Rev. Lett. **68**, 2830 (1992); Phys. Rev. B **47**, 7995 (1993).
[23] R. Fazio and D. Zappala, Phys. Rev. B **53**, R8883 (1996).
[24] M. Jarrell and J. E. Gubernatis, Phys. Rep. **269**, 133 (1996).
[25] W. H. Press *et al.*, *Numerical Recipes in C* (Cambridge University Press, Cambridge, England, 1992).
[26] See Y. Liu *et al.*, Physica (Amsterdam) **83D**, 163 (1995), and references therein.
[27] *Finite Size Scaling and Numerical Simulations of Statistical Systems*, edited by V. Privman (World Scientific, Singapore, 1990).